# Extreme Masking for Learning Instance and Distributed Visual Representations

**Anonymous authors**
**Paper under double-blind review**

## Abstract

The paper presents a scalable approach for learning distributed visual representations over individual tokens and a holistic instance representation simultaneously. We use self-attention blocks to represent spatially distributed tokens, followed by cross-attention blocks to aggregate the holistic instance. The core of the approach is the use of extremely large token masking (75%-90%) as the data augmentation for supervision. Our model, named ExtreMA, follows the plain BYOL approach where the instance representation from the unmasked subset is trained to predict that from the intact input. Learning requires the model to capture informative variations in an instance, instead of encouraging invariance.

The paper makes three contributions: 1) It presents random masking as a strong and computationally efficient data augmentation for learning generalizable attention representations. 2) With multiple sampling per instance, extreme masking greatly speeds up learning and creates hunger for more data. 3) Distributed representations can be learned from instance supervision alone, unlike per-token supervision in masked modeling.

## 1 Introduction

Masked modeling (Devlin et al., 2018) has emerged as a viable approach for visual representation learning. On a generic transformer architecture (Vaswani et al., 2017), it optimizes a learning objective based on the masked signal prediction popularized in natural language understanding (Devlin et al., 2018; Liu et al., 2019), without reliance on heavily engineered image augmentations (Wu et al., 2018; Chen et al., 2020b; Grill et al., 2020). Superior finetuning performance has been demonstrated with this approach; however, the pretrained representation does not work competitively off-the-shelf (Bao et al., 2021), e.g., for k-nearest-neighbor retrieval.

On the other hand, Siamese networks trained with contrastive objectives (Oord et al., 2018) are strong for learning off-the-shelf representations (Radford et al., 2021). This fundamental difference lies in the way they represent data. Siamese networks extract an instance representation for an image, whereas masked modeling acquires a spatially distributed representation (Mikolov et al., 2013) over individual tokens that comprise an image. No instance representation is explicitly modeled or provided supervision in masked modeling approaches (Devlin et al., 2018; Bao et al., 2021).

In this paper, we study the connections between the instance and the distributed representations, and we explore self-supervision for learning these representations. We start with an observation that random masking could be viewed as a novel data augmentation scheme not previously exploited in Siamese networks. For the masked area, its potential degrees of freedom grow combinatorially large with its size, allowing for richer self-supervision than conventional augmentations such as cropping and scaling, which are heavily biased towards areas around the image center (He et al., 2021). More importantly, the self-supervision from conventional augmentations lead to a common representation vector that encompasses multiple augmentations of an instance, and this invariance degrades the sensitivity of the representation to spatial locality. On the contrary, random masking preserves the original content of the unmasked area and the geometrical structure of the data.

We propose a simple model, called ExtreMA, where the instance representation from masked input is trained to predict that from the full view, in a plain BYOL fashion (Grill et al., 2020). The information gap created by masking encourages the student network to encode as much information as possible, and hence bootstrap the teacher network to be stronger. We adopt the visual transformer ViT (Dosovitskiy et al., 2020) to embed distributed representations over patches, and this is followed by cross-attention blocks (Touvron et al., 2021b) to aggregate the distributed representations into the instance representation. The instance-level learning objective provides the supervision for both of the representations. In our model, the distributed representations are only implicitly learned without the corresponding token-level objective used in masked modeling. However, through investigating and visualizing the attention maps (in Figure 1), we find that the output representations of our model maintain accurate correspondences with the input tokens and that semantic clusters tend to emerge from the learned distributed representations.

A notable distinction of this model is its effectiveness with an extremely large masking ratio (75% - 90%), while typical masked modeling approaches work best between the range of 50% to 75% (El-Nouby et al., 2021; Bao et al., 2021; He et al., 2021). Besides the computational efficiency that this brings, a key aspect of extreme masking is the complementarity that arises among multiple samples. Due to the high redundancy in visual data, the visible content for samples with different masking becomes independent only when the masking ratio becomes large. In addition, multiple masks speed up learning and convergence significantly, making the system a fast learner that is hungry for more data. In practice, multiple sampling is also computationally appealing, as the teacher network for processing the full content needs only to be forwarded once.

ExtreMA enjoys the favorable properties of Siamese representation learning. The instance representation from the model can be used off-the-shelf for measuring semantic similarities. The framework also welcomes other data augmentations besides masking for applications with different ends. However, unlike conventional contrastive learning, ExtreMA does not rely on data augmentation induced invariances to achieve generalization. Rather, ExtreMA preserves all possible useful information from the masked view in order to recover the full image. The generative aspects of our model are exhibited in Figure 2. It can faithfully inpaint the masked pixels through network inversion (Zhao et al., 2020b). Moreover, the instance representation is shown to be sensitive to spatial and scale variations for localizing objects in Figure 3. These properties demonstrates that ExtreMA learns both instance and distributed representations that well captures scale, location, and color intensities.

In the experiments, we systematically study the model behavior under different masking ratios, its convergence properties using multiple masks on larger datasets, and integration with various other data augmentations. Based on the study observations, we also propose a new augmentation scheme which uses shared image crops but different colors for the two input views. Our main results on ImageNet1k outperform prior masked modeling approaches on both finetuning and linear probing metrics. Notably, this is achieved by training ExtreMA using a single node of 8×V100 GPUs in about two days for a ViT-Base model. We also evaluate the transfer performance for semi-supervised learning and semantic segmentation. For both applications, ExtreMA produces superior results compared with prior arts.

## 2 Related Works

In self-supervised representation learning, labels are mined from the data itself to achieve generalization beyond that from human annotations, especially when the training data is at scale. Past works demonstrate generalization through k-nearest-neighbors (Wu et al., 2018) and zero-shot classification on the learned features (Radford et al., 2021), or finetuning the model for a limited schedule (Chen et al., 2020c; He et al., 2021). The central problem under investigation is how to extract the training labels automatically and formulate the pretext tasks. In high-level vision, such pretext tasks include predicting colors from a grayscale image (Zhang et al., 2016), inpainting pixels given the spatial context (Doersch et al., 2015) or through autoregression (Chen et al., 2020a), predicting the orientation of a rotated image (Gidaris et al., 2018), solving a jigsaw puzzle given shuffled patches (Noroozi & Favaro, 2016), and others (Donahue & Simonyan, 2019; Zhang et al., 2017). The key idea is that the network has to learn semantics in order to solve the pretext tasks. Recently, there has been a resurgence of the context prediction pretext task (Bao et al., 2021; Li et al., 2021b) that has accompanied the rise of visual transformers (Dosovitskiy et al., 2020). Input tokens are

masked, and the model is trained to predict the masked tokens from the visible tokens in a BERT fashion. The target tokens could be represented by dVAE tokens (Bao et al., 2021), raw pixel values (He et al., 2021), or features (Wei et al., 2021; Dong et al., 2021) from an online learned encoder (Zhou et al., 2021; El-Nouby et al., 2021; Baevski et al., 2022; Chen et al., 2022; Tao et al., 2022). Such representations are shown to surpass prior art when finetuned for downstream tasks (He et al., 2021).

Contrastive learning is a special pretext task of instance discrimination to learn view-invariant representations from data augmentations. It encourages different views of an image instance to have similar representations relative to negative samples (Wu et al., 2018; He et al., 2020; Chen et al., 2020a), negative clusters (Caron et al., 2020), or even without using negatives (Grill et al., 2020) at all. Views of an image are commonly processed by a Siamese network (Chen et al., 2020b; Li et al., 2021a) with a momentum encoder (He et al., 2020) on one of its branches. To boost performance, the community has crafted various data augmentations including color jittering (Wu et al., 2018), Gaussian blurring (Chen et al., 2020b), solarization (Grill et al., 2020), and copy-and-paste (Zhao et al., 2020a), as well as determined their optimal hyper-parameters. Contrastive models trained at scale are shown to perform on par with supervised learning (Goyal et al., 2019; 2021). The contrastive learning framework has the flexibility to handle various data augmentations, while traditional pretext tasks need non-trivial engineering to be trained in a multi-task manner (Doersch & Zisserman, 2017). Recently, there have been efforts (El-Nouby et al., 2021; Zhou et al., 2021) to combine contrastive learning with masked modeling objectives in a multi-task manner. The two tasks complement each other, but the intrinsic connection remains unclear.

The technique of masking originates from representation learning on languages (Devlin et al., 2018; Liu et al., 2019) and is especially suited for transformer architectures. In computer vision, block-wise masking (Bao et al., 2021) and random masking (He et al., 2021) are investigated to cope with the 2D nature of images. Aside from BERT-like training approaches (Bao et al., 2021; He et al., 2021; El-Nouby et al., 2021; Zhou et al., 2021; Baevski et al., 2022), a special type of random masking in the form of small local image crops has also been adopted in contrastive models (Caron et al., 2021; 2020). However, the local crop augmentation introduced in (Caron et al., 2020) is mainly designed for computational efficiency, without revealing the impact of substantial content removal on representation quality. A recent work MSN (Assran et al., 2022) explores the application of masking in Siamese networks. However, its masking ratio is low (30% for ViT-base), and it heavily relies on other augmentations besides masking to work. Data2vec (Baevski et al., 2022) exploits a similar Siamese network architecture for representation learning, but its supervision is applied for each token as in masked modeling. Hybrid models (Zhou et al., 2021; Tao et al., 2022) of contrastive learning and masked image modeling formulate a multi-task problem to enjoy the best of two paradigms. However, the technique of masking is mainly to supervise masked modeling, not as an augmentation for contrastive learning. Specifically, Zhou et al. (2021) finds that adding masking augmentation actually hurts representation quality. Our work reveals the power of masking even when used as a data augmentation, without explicit supervision for token-level predictions.

## 3 The ExtreMA Approach

This work explores the use of random masking as data augmentation for Siamese representation learning with instance-level supervision. The model uses an architecture of two parallel networks, where the momentum encoder processes the full image crop and the base encoder processes the masked image crop. The information gap, i.e. the masked image region, is the basis of the supervision for training the base encoder. An overview of our approach is illustrated in Figure 1. We describe details about masking and the model architecture as follows.

**Extreme Masking.** Given an image, we first divide it into non-overlapping patches to be fed into the visual transformer. A fixed sinusoidal positional encoding is added to each embedded patch, and a few of the embedded patches are sampled randomly (He et al., 2021) according to the masking ratio.

A key aspect of our approach is that it achieves its best performance with an extremely large masking ratio of 75%-90%, leaving the base encoder to process just a fraction (10%-25%) of the patches. This is in contrast to masked image modeling where the performance degrades when the masking ratio exceeds 75% (He et al.,

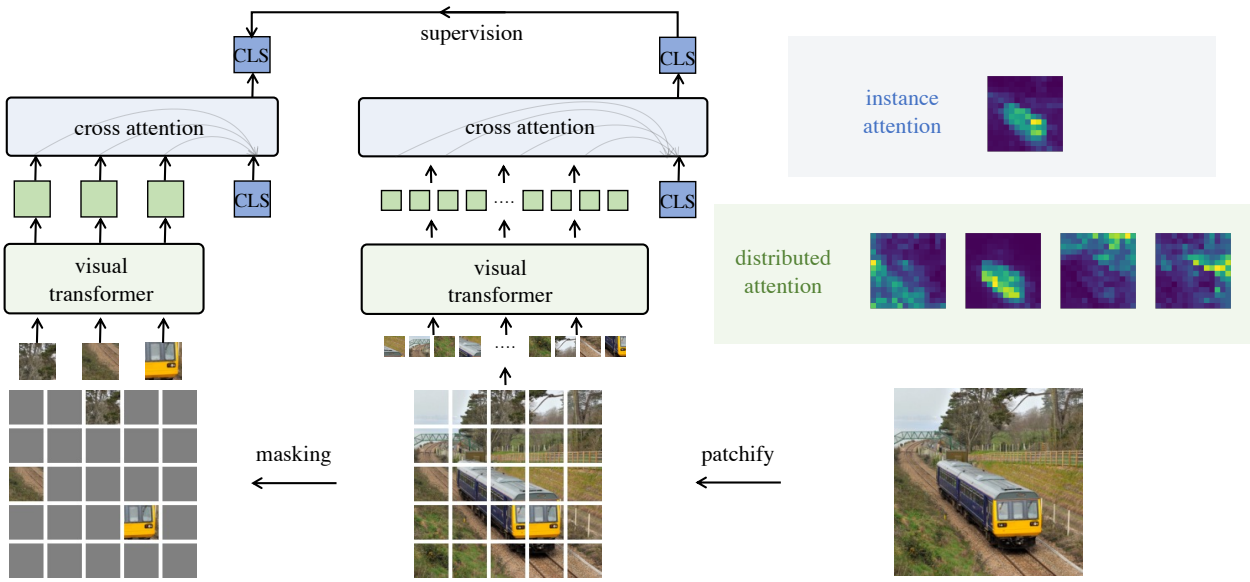


Figure 1: **Overview of ExtreMA.** Our model follows the Siamese network approach for representation learning. The momentum encoder processes the full view while the base encoder processes a partial view from extreme masked sampling. Input tokens are encoded into distributed representations via visual transformers and gathered into an instance representation via cross-attention blocks with an appended $[CLS]$ token. Self-supervision is applied at the instance level. We visualize attention maps for four query patches in the last layer of ViT and cross attention for the class token.

2021). The extremely high masking ratio sets a very hard pretext task for the network. The ability of ExtreMA to succeed with extreme masking is in part due to the momentum encoder processing the entire image, whereas the encoder in the masked image modeling never receives the full view as input. This creates train-test discrepancy for masked modeling, as the attention blocks need to generalize from processing a fraction of the tokens to the full set.

Extreme masking provides two other critical benefits. First, a very large masking ratio leads to independent and complementary views from the same image. This allows us to use a batch of masks for learning, significantly expediting learning and convergence. Second, extreme masking substantially reduces the computation cost for the base encoder, especially for transformers which have squared complexity. When multiple masks per instance (multi-masking) are used, multiple student networks can share the same learning target from the momentum encoder. This makes extreme masking an efficient learner. We note that such a multi-masking technique is not immediately applicable or efficient for masked modeling since different masks do not share the same target.

Extreme masking also introduces new challenges. The space of masking augmentations becomes combinatorially smaller when the masking ratio increases. In practice, we observe that extreme masking tends to overfit to the training data especially when multi-masking is enabled. This is different from "cheating", as the feature effectively learns semantics on the training data. The overfitting phenomenon simply suggests that extreme masking is hungry for more training data. This is discussed further in the experiments section.

**Distributed and Instance Representations.** We adopt the vision transformer (Dosovitskiy et al., 2020) for its efficiency and flexibility in handling input content of variable size. The vision transformer embeds the input visual tokens into a spatially distributed representation via the self-attention mechanism. An instance representation is desired in order to allow supervision from the instance level. To achieve this, we use cross-attention blocks (Touvron et al., 2021b) to aggregate the distributed patch-level representations into a single representation with an additional appended class token. The distributed representations are frozen without updates, and this makes the cross-attention blocks lightweight with O(N) complexity compared to O($N^2$) in self-attention. The projection head and the predictor follow the instance representation.

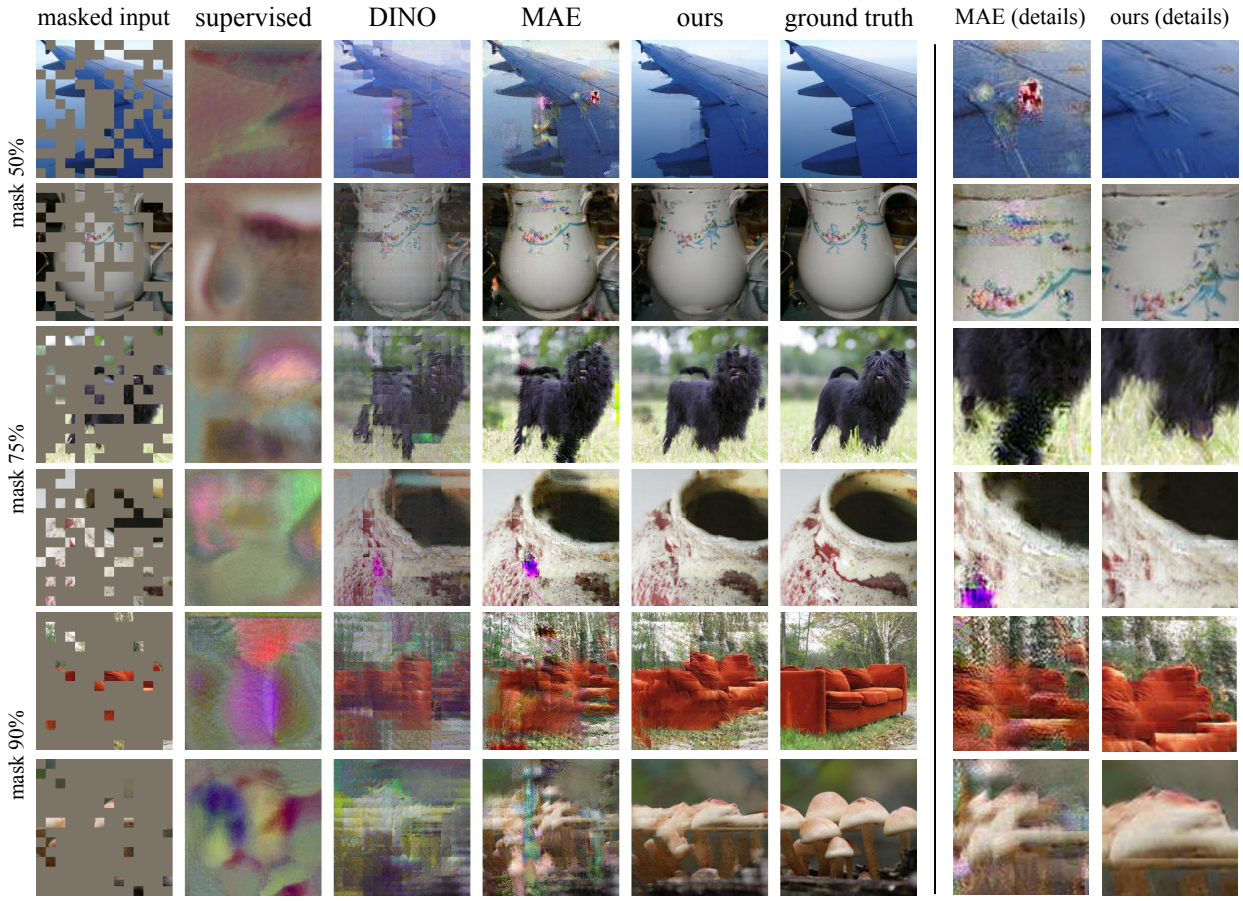


Figure 2: **Generative properties of the distributed representations at various masking ratios.** We use the deep image prior technique to invert the representations. Our reconstruction result shows the best quality overall. Supervised ViT fails to produce meaningful content. MAE fails to inpaint proper colors due to the use of normalized pixels. DINO loses information about spatial locality.

We have investigated two other alternatives to represent an instance, but neither works well. If we feed the instance token as an input to the transformer as in ViT, optimization becomes unstable, potentially due to the large masking rate for the input. With average pooling over the token representations as the instance representation, the model finds a shortcut on learning averaged patch features without learning attention across patches. Details are provided in the appendix.

**Learning Objective.** The instance representation from the masked input is trained to predict that from the unmasked input by simply minimizing the cosine distance between the two representations. We primarily follow BYOL for simplicity in this paper, but our approach is also found to work with the contrastive loss (Wu et al., 2018; Oord et al., 2018) in our experiments. Our learning objective differs with the conventional BYOL in the following aspect. Conventional BYOL adopts a symmetric loss where the two views are learned to predict each other. This will drive the representation to find the common subspace shared by the two views, with invariance over other information (Tian et al., 2020). In our case, since the shared information between the two views is obvious, finding the commonality between the views does not make for meaningful self-supervision. Thus, we adopt the asymmetric loss. The information gap created by masking encourages the network to extrapolate the masked regions, instead of seeking a shared subspace.

Compared with masked modeling approaches, our learning objective is fundamentally different. The instance level supervision does not explicitly enforce spatial reasoning for each individual token. Nonetheless, we find strong evidence that our model learns a distributed representation over the tokens. We visualize the attention maps for four query patches in the last layer of the transformer block in Figure 1. The shown visualization is

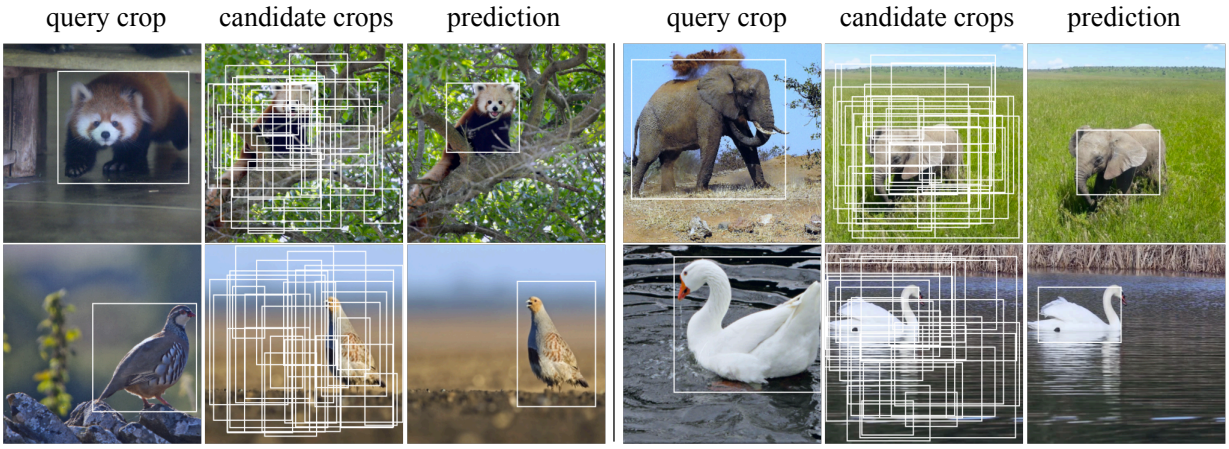


Figure 3: **ExtreMA is sensitive to spatial and scale variations.** We randomly sample 25 candidate bounding boxes of 5 scales and 5 random locations from a test image and we use the query crop to retrieve the closest bounding box in the test image. The highest ranked crop is shown as the prediction. The instance representation from our model is able to identify the correct scale and location, suggesting that ExtreMA is sensitive to information beyond semantics.

averaged across 12 attention heads. We observe that patch tokens tend to group into meaningful semantic clusters.

**BYOL Details.** Our design choices for the projection and the prediction head are even simpler than the original BYOL (Grill et al., 2020). We replace the BatchNorm with LayerNorm and the ReLU activations with GeLU activations, making the overall framework free of BatchNorm and consistent with the rest of the transformer blocks. Our work also incidentally demonstrates that BYOL does not rely on BatchNorm to prevent collapse (Richemond et al., 2020). The projection head and the prediction head have 3 and 2 hidden layers respectively, a hidden dimension of 4096, and an output dimension of 256, following the original design.

## 4 Representation Properties

To understand the distributed representation and the instance representation trained with extreme masking augmentation, we invert the distributed representations into the pixel space and examine the sensitivity to locality of the instance representation. These results give further evidence that the model learns a meaningful distributed representation without a BERT-like objective, and that the instance representation preserves detailed visual information. The following analysis is not meant to compare different models in a quantitative way, but to provide intuitive insights on what have been learned by the models.

**Generative Properties.** Given a pretrained model and a masked image, we can encode the visible patches using the distributed representations, and invert these partial representations back to the pixel space to reconstruct the masked patches. Specifically, we follow the technique of deep image prior (Ulyanov et al., 2018) and minimize the L2 distance on the visible representations between the masked image and the reconstruction. This reconstruction technique allows us to examine the content of the encoded features without the need to further train a new generative model. Figure 2 shows the reconstruction result. We vary the masking ratio and compare results with supervised DeiT (Touvron et al., 2021a), DINO and MAE [1] using this inversion method. Supervised DeiT is unable to produce any meaningful content. MAE fails to inpaint proper colors due to the use of normalized pixels. DINO is inaccurate with spatial localities. Our result is spatially smooth and accurate in color. The inversion technique suffers when the masking ratio is very large, due to limited ability to inpaint unseen semantic areas.

[1]We acknowledge that MAE is able to do amazing reconstruction using its decoder. The inversion experiment for MAE is mainly to investigate its encoder in a fair comparison with competing approaches.

Table 1: Mask ratio.

| ratio | ft. | lin. |
|---|---|---|
| 50% | 81.9 | 36.3 |
| 70% | 82.3 | 64.4 |
| 80% | 82.4 | 67.3 |
| 85% | 82.4 | 66.3 |
| 90% | 82.3 | 61.6 |
| 95% | 81.6 | 49.3 |

Table 2: Multi-masks trained on IM1k.

| ratio 75% | | | ratio 80% | | | ratio 90% | | |
|---|---|---|---|---|---|---|---|---|
| num | ft. | lin. | num | ft. | lin. | num | ft. | lin. |
| 1 | 82.4 | 64.8 | 1 | 82.4 | 67.3 | 1 | 82.3 | 61.6 |
| 2 | 82.7 | 67.2 | 2 | 82.6 | 68.8 | 2 | 82.5 | 64.0 |
| 4 | 82.9 | 67.7 | 4 | 82.8 | 67.5 | 4 | 82.7 | 63.1 |
| | | | 5 | 82.9 | 67.1 | 8 | 82.9 | 60.3 |
| | | | | | | 10 | 83.0 | 59.3 |

Table 3: Trained on IM22k.

| ratio 90% | | |
|---|---|---|
| num | ft. | lin. |
| 1 | 82.5 | 60.4 |
| 2 | 82.7 | 65.6 |
| 4 | 83.0 | 69.0 |
| 8 | 83.2 | 71.4 |
| 10 | 83.2 | 72.0 |

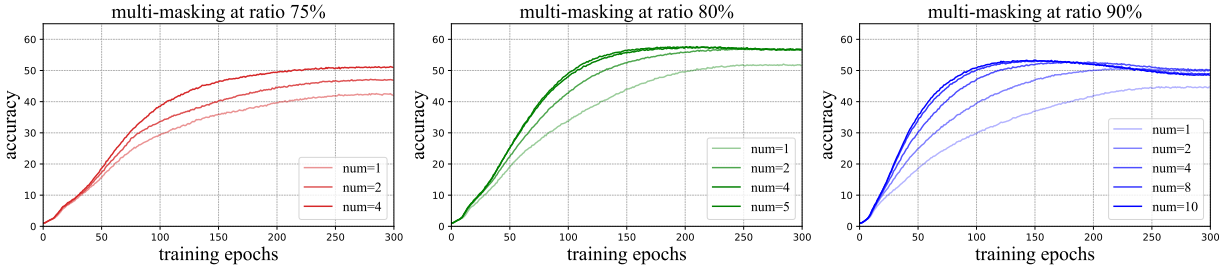


Figure 4: Convergence curves for multi-masking on ImageNet1k. Each plot shows kNN accuracy on the validation set with respect to training epochs. Multi-masking with 80% and 90% ratio enjoys steep learning curves, but suffers from overfitting on ImageNet1k.

**Locality Properties.** We use the k-nearest neighbor technique to probe the instance representation. We first generate a small gallery set by random sampling of image crops that vary spatially and in scale from a single image. We then use another query image crop from the same semantic category to rank the gallery set. We resize these image crops to $224 \times 224$ and extract the instance representations for measuring similarities. In Figure 3, the top nearest retrieval returns the image bounding box with the closest spatial and scale configuration as the query crop. The results suggest that the instance representation is sensitive to spatial and scale changes, and the learned high-level representation is not a result of invariance but is more powerful and generalizable. This example also demonstrates a form of zero-shot detection using exemplars (Malisiewicz et al., 2011).

## 5 Experiments

### 5.1 Ablation Studies

We pretrain the representation on ImageNet and evaluate it on finetuning (ft) and linear probe (lin) in our ablations. We finetune the model on top of the distributed representation, and conduct linear probes with the instance representation. The evaluation protocol mainly follows BEiT and MAE.

**Implementation Details**. We use the original ViT-base (Dosovitskiy et al., 2020) as the backbone architecture without the layer scale technique (Touvron et al., 2021b). The class attention follows the original design in (Touvron et al., 2021b) with a default of two transformer blocks and a layer scale hyper-parameter of 0.1. We train our model using the AdamW optimizer (Loshchilov & Hutter, 2017) with a batch size of 2048, an initial base learning rate of 1.5e-4, and a weight decay of 0.1. The exponential averaging weight for the momentum encoder is initialized to 0.996 and increased to 1.0 following a cosine schedule. The default augmentation is random resized cropping and random flipping. All models are trained for 300 epochs.

**Masking Ratio.** We first vary the masking ratio using a single mask for training. In Table 1, the finetuning performance plateaus across a wide range from 70% to 90%, while the linear probe performance peaks at ratio 80%. Notably, an extremely large masking ratio of 90% also achieves reasonably good performance. The performance degrades beyond 90%.

**Multi-Masking and Convergence Speed.** For each image instance, we generate multiple masks without replacement for the student network. The loss is averaged over multiple masked inputs. We investigate

Table 4: Other augmentations.

| augment | 1 aug | | 2 augs | |
|---|---|---|---|---|
| | ft. | lin. | ft. | lin. |
| none | 82.3 | 55.1 | - | - |
| color | 82.5 | 62.0 | 83.3 | 62.4 |
| rand size crop | 82.6 | 68.8 | 82.2 | 66.8 |
| crop + color | 82.6 | 69.0 | 83.1 | 73.3 |
| shared crop + color | - | - | 83.3 | 73.1 |

Table 5: Cross attention block.

| #blocks | ft. | lin. |
|---|---|---|
| 1 | 82.6 | 66.2 |
| 2 | 82.6 | 68.8 |
| 3 | 82.6 | 68.5 |

Table 6: Training loss.

| objective | ft. | lin. |
|---|---|---|
| BYOL | 82.6 | 68.8 |
| InfoNCE | 82.8 | 66.8 |

the behavior of multi-masking under the ratios of 75%, 80%, and 90% in Table 2. Finetuning performance consistently improves with more masked inputs. However, the linear probe performance degrades when too many masks are used, especially when the masking ratio gets larger. We take a close look at this phenomenon and find that the training accuracy for linear probing actually improves with greater multi-masking. This suggests that the model overfits to the training data without using labels. In Figure 4, we plot the k-nearest-neighbor classification curves on the validation set with respect to training epochs. The hyper-parameter $k$ is set to 200 and the gallery is set to 10% of the ImageNet training set. Masking with ratio 75% does not suffer from overfitting with multi-masking, but converges less quickly. Multi-masking with extreme ratio 90% has the steepest learning curve, but it tends to saturate and degrade after 120 epochs. We hypothesize that this is due to the complexity of the masking augmentation, which may decrease as the masking ratio grows.

To combat overfitting while preserving fast learning, a straightforward solution is to use larger datasets. We therefore study multi-masking on ImageNet22k, which is about 10 times larger in total images. We train the model for 30 epochs, which maintains the effective number of optimization iterations and reveals the impact solely from data scale. The evaluations for finetuning and linear probing are all conducted with ImageNet1k. In Table 3, at the masking ratio of 90%, ExtreMA no longer suffers from overfitting as the number of masks increases. The model performance is also consistently better than using ImageNet1k training data. This shows that our model wants more data and benefits from large-scale representation learning.

**Other Augmentations.** Supervision at the instance level enables integration of other augmentations for both the student and teacher networks. We set the default masking ratio to 80% with two masks in the following ablations, as it does not suffer from overfitting. We consider the augmentations of cropping (random resized crop + flipping) and color (color jittering and random grayscaling). We do not consider Gaussian blurring and solarization as their effects are marginal.

We first examine the case of a single augmentation, where the input of the teacher branch is augmented and the student branch takes a random masking sample of the teacher's input. Such a scheme is akin to enlarging the training dataset without introducing other supervision from augmentations. As reported in Table 4, by just using a center crop, our model achieves a reasonable result of 82.3% finetuning and 55.1% linear probing performance. Color and cropping augmentations improve the overall performance individually but their effects are marginal when both are used.

We next consider two independent augmentations, one for the student and one for the teacher, with the student's input undergoing masking as well. The self-supervision in such a scheme introduces invariance, such as spatial, scale, and color intensity, similar to prior contrastive models (Caron et al., 2021; Chen et al., 2021). Crucially, we find that adding spatial and scale invariance by two crops of an image may hurt representation quality, with finetuning decreased by 0.4% and linear probing decreased by 2.0%. On the other hand, color invariance is shown to be beneficial, leading to a significant 0.8% gain from 82.5% to 83.3%. Using cropping and color augmentations combined, the linear probing performance improves substantially to 73.3% while the finetuning performance drops 0.2% as spatial invariance may hurt generalization.

Based on these observations, we propose another augmentation scheme that uses a shared spatial crop for the two network branches, but two different color augmentations. Such scheme achieves the best overall performance for finetuning and linear probing.

Table 7: ImageNet1k classification comparison.

| methods | epochs | ViT-S | | ViT-B | |
|---|---|---|---|---|---|
| | | ft. | lin. | ft. | lin. |
| MoCo-v3 | 300 | 81.5 | 73.1 | 83.2 | 76.2 |
| DINO | 400 | 81.7 | **77.0** | 83.6 | **78.2** |
| BEiT | 800 | - | - | 83.2 | 37.6 |
| MAE | 1600 | - | - | 83.6 | 67.8 |
| ExtreMA (1k) | 300 | **81.8** | 69.4 | **83.7** | 73.3 |
| ExtreMA (22k) | 30 | 81.5 | 65.7 | **83.9** | 74.5 |

Table 8: ViT-B Wall-clock time comparison using a single node of 8×V100 GPUs.

| methods | epochs | time |
|---|---|---|
| DINO | 400 | 300 hrs |
| BEiT | 800 | 240 hrs |
| MAE | 1600 | 650 hrs |
| ExtreMA (80% ratio ×1) | 300 | 29 hrs |
| ExtreMA (80% ratio ×2) | 300 | 36 hrs |
| ExtreMA (80% ratio ×5) | 300 | 60 hrs |

**Cross Attention Blocks.** We use cross-attention heads (Touvron et al., 2021b) to aggregate the distributed representations into the instance representation. We ablate the number of blocks for this design in Table 5. The finetuning performance is not affected by the depth of the cross-attention blocks, while the linear probing performance is improved by 2% with two blocks and saturates for more blocks.

**Training Objective.** Besides BYOL, ExtreMA also works with other Siamese representation learning objectives, such as InfoNCE (Oord et al., 2018) with negatives. In Table 6, we provide the result with a MoCo-v3 implementation using a contrast temperature of 0.2. Compared with the BYOL objective, the finetuning performance is improved by 0.2% and linear probing drops by 2.0%.

### 5.2 ImageNet Comparisons with Previous Methods

We compare with representative contrastive methods MoCo-v3 and DINO, as well as masked image modeling methods BeiT and MAE on ImageNet classification. We use our strongest model with five masks of ratio 80% and color augmentations. The finetuning takes 200 epochs for ViT-S and 100 epochs for ViT-B following prior works. The results are summarized in Table 7. Our approach achieves the best finetuning performance for both architectures. Our linear probing outperforms the masked image modeling methods by a large margin but underperforms contrastive counterparts. This may be due to the lack of global crops and other heavy image augmentations. The ViT-S model does not scale well with large data, potentially limited by its model size.

A notable advantage for ExtreMA is its computational efficiency and fast convergence speed. This allows us to train ViT-Base models of 300 epochs using a single node of 8×V100 GPUs for 29 hours to 60 hours depending on the choice of multi-masking. Such hardware requirement is amenable to resource-limited academic labs. On the contrary, prior self-supervised representation models require multi-node training and lengthy optimization. We summarize the wall clock times of representative models in Table 8. Since official releases of prior methods are reported with multi-node training, we estimate their wall-clock time using just a single node of 8×V100 GPUs. ExtreMA achieves 5× to 10× speedups for visual representation learning.

### 5.3 Transfer Learning Results

We consider two transfer learning scenarios with limited target labels: semi-supervised image classification and semantic segmentation. For both experiments, we use our strongest model with five masks of ratio 80% and color augmentations.

**Semi-supervised Learning.** Given the pretrained model, we use a small fraction of the ImageNet1k training labels (1% or 10%) for semi-supervised finetuning. We append the classification head on the first output layer of the projection head following SimCLR-v2 Chen et al. (2020c). The finetuning protocol and data augmentation mainly follows BEiT. The model is optimized using AdamW with an initial learning rate of 5e-6 for 1000 epochs and a batch size of 1024. Comparison results are shown in Table 10. ExtreMA outperforms the masked image modeling approaches MAE and BEiT by a large margin of 12% and 30% using 1% of the labels. Surprisingly, ExtreMA obtains better results than DINO, which is heavily tuned for ImageNet classification with higher linear probing performance than our approach. The models pretrained

Table 9: Semantic segmentation on ADE20K.

| methods | epochs | mIoU |
|---|---|---|
| DINO | 300 | 47.2 |
| MoCo-v3 | 300 | 47.3 |
| BEiT | 800 | 47.1 |
| MAE | 1600 | **48.1** |
| ExtreMA (1k) | 300 | 47.9 |
| ExtreMA (22k) | 30 | **48.4** |

Table 10: Semi-supervised classification.

| methods | epochs | 1% | 10% |
|---|---|---|---|
| scratch | - | 9.0 | 44.8 |
| BEiT | 800 | 35.9 | 69.7 |
| DINO | 400 | 64.7 | 75.9 |
| MoCo-v3 | 300 | 57.2 | 75.8 |
| MAE | 1600 | 52.7 | 72.1 |
| ExtreMA (1k) | 300 | **67.3** | **76.1** |

Table 11: Object detection and instance segmentation transfer on COCO.

| methods | epochs | object detection | | | instance segmentation | | |
|---|---|---|---|---|---|---|---|
| | | $AP$ | $AP_{50}$ | $AP_{75}$ | $AP$ | $AP_{50}$ | $AP_{75}$ |
| DINO | 300 | 46.8 | 68.6 | 50.9 | 41.5 | 65.3 | 44.5 |
| MoCo-v3 | 300 | 45.5 | 67.1 | 49.4 | 40.5 | 63.7 | 43.4 |
| BEiT | 800 | 42.1 | 63.3 | 46.0 | 37.8 | 60.1 | 40.6 |
| MAE | 300 | 45.4 | 66.4 | 49.6 | 40.6 | 63.4 | 43.7 |
| MAE | 1600 | 48.4 | 69.4 | 53.1 | 42.6 | 66.1 | 45.9 |
| ExtreMA (1k) | 300 | 47.5 | 68.9 | 51.9 | 42.0 | 65.6 | 45.1 |
| ExtreMA (22k) | 30 | **48.5** | **69.8** | **53.1** | **42.7** | **66.5** | **46.0** |

with ImageNet22k perform worse, because the majority of unlabeled classes are less relevant to the target 1k classes. We thus follow the prior evaluation practice and omit the ImageNet22k entry.

**Semantic Segmentation.** We evaluate semantic segmentation performance on the ADE20K (Zhou et al., 2017) dataset. Following prior works, we initialize the UperNet framework (Xiao et al., 2018) using our pretrained model and finetune the segmentation model end-to-end. The model is optimized using AdamW for 80k iterations with an initial learning rate of 1e-4 and a batch size of 16. We set the weight decay to 0.05 and layer-wise learning rate decay to 0.85. The results are shown in Table 9. Our method is able to outperform competitive representation learning baselines such as DINO, MoCo-v3 and BEiT. Our model is even comparable to MAE, which is trained with a much heavier schedule (300 epochs vs. 1600 epochs). By scaling the training data to the larger ImageNet-22K dataset while keeping the total number of iterations unchanged, our model performance improves by 0.5 mIoU, surpassing all prior arts by a significant margin. This indicates that our model scales well with data.

**Object Detection and Instance Segmentation.** We evaluate the transfer performance on the MSCOCO dataset. We adopt the Mask-RCNN framework for object detection and instance segmentation using the ViT-base architecture. We fine-tune the model for 12 epochs and evaluate the performance on the validation set. The results are summarized in Table 11. ExtreMA outperforms DINO/MoCo-v3/BEiT while using a lot less compute. ExtreMA outperforms MAE with the same number of pretraining epochs, but underforms MAE if MAE is trained longer. When pretrained on the ImageNet22k dataset, ExtreMA improves the performance by about 1% AP.

## 6 Conclusions

This work explores masking as a novel augmentation for Siamese representation learning. The investigated approach, ExtreMA, learns strong instance and distributed representations through data augmentations without masked modeling supervision. This work is inspired by the masking operation in masked modeling. However, it makes no claims that ExtreMA works in a similar way as masked modeling, since the learning objectives are different. ExtreMA exhibits several unique characteristics: 1) the use of extremely large masking ratios, 75%-90%; 2) fast convergence speed with multi-masking and scalability to large data; 3) low consumption of computational resources. Its ability on encoding precise locality for the instance representation may open up a new possibility for detection transfer.

## References


Mahmoud Assran, Mathilde Caron, Ishan Misra, Piotr Bojanowski, Florian Bordes, Pascal Vincent, Armand Joulin, Michael Rabbat, and Nicolas Ballas. Masked siamese networks for label-efficient learning. *arXiv preprint arXiv:2204.07141*, 2022.

Alexei Baevski, Wei-Ning Hsu, Qiantong Xu, Arun Babu, Jiatao Gu, and Michael Auli. Data2vec: A general framework for self-supervised learning in speech, vision and language. *arXiv preprint arXiv:2202.03555*, 2022.

Hangbo Bao, Li Dong, and Furu Wei. Beit: Bert pre-training of image transformers. *arXiv preprint arXiv:2106.08254*, 2021.

Mathilde Caron, Ishan Misra, Julien Mairal, Priya Goyal, Piotr Bojanowski, and Armand Joulin. Unsupervised learning of visual features by contrasting cluster assignments. *Advances in Neural Information Processing Systems*, 33:9912–9924, 2020.

Mathilde Caron, Hugo Touvron, Ishan Misra, Hervé Jégou, Julien Mairal, Piotr Bojanowski, and Armand Joulin. Emerging properties in self-supervised vision transformers. In *Proceedings of the IEEE/CVF International Conference on Computer Vision*, pp. 9650–9660, 2021.

Mark Chen, Alec Radford, Rewon Child, Jeffrey Wu, Heewoo Jun, David Luan, and Ilya Sutskever. Generative pretraining from pixels. In *International Conference on Machine Learning*, pp. 1691–1703. PMLR, 2020a.

Ting Chen, Simon Kornblith, Mohammad Norouzi, and Geoffrey Hinton. A simple framework for contrastive learning of visual representations. In *International conference on machine learning*, pp. 1597–1607. PMLR, 2020b.

Ting Chen, Simon Kornblith, Kevin Swersky, Mohammad Norouzi, and Geoffrey E Hinton. Big self-supervised models are strong semi-supervised learners. *Advances in neural information processing systems*, 33: 22243–22255, 2020c.

Xiaokang Chen, Mingyu Ding, Xiaodi Wang, Ying Xin, Shentong Mo, Yunhao Wang, Shumin Han, Ping Luo, Gang Zeng, and Jingdong Wang. Context autoencoder for self-supervised representation learning. *arXiv preprint arXiv:2202.03026*, 2022.

Xinlei Chen, Saining Xie, and Kaiming He. An empirical study of training self-supervised vision transformers. In *Proceedings of the IEEE/CVF International Conference on Computer Vision*, pp. 9640–9649, 2021.

Jacob Devlin, Ming-Wei Chang, Kenton Lee, and Kristina Toutanova. Bert: Pre-training of deep bidirectional transformers for language understanding. *arXiv preprint arXiv:1810.04805*, 2018.

Carl Doersch and Andrew Zisserman. Multi-task self-supervised visual learning. In *Proceedings of the IEEE International Conference on Computer Vision*, pp. 2051–2060, 2017.

Carl Doersch, Abhinav Gupta, and Alexei A Efros. Unsupervised visual representation learning by context prediction. In *Proceedings of the IEEE international conference on computer vision*, pp. 1422–1430, 2015.

Jeff Donahue and Karen Simonyan. Large scale adversarial representation learning. *Advances in Neural Information Processing Systems*, 32, 2019.

Xiaoyi Dong, Jianmin Bao, Ting Zhang, Dongdong Chen, Weiming Zhang, Lu Yuan, Dong Chen, Fang Wen, and Nenghai Yu Peco. Perceptual codebook for bert pre-training of vision transformers. *arXiv preprint arXiv:2111.12710*, 1(3):7, 2021.

Alexey Dosovitskiy, Lucas Beyer, Alexander Kolesnikov, Dirk Weissenborn, Xiaohua Zhai, Thomas Unterthiner, Mostafa Dehghani, Matthias Minderer, Georg Heigold, Sylvain Gelly, et al. An image is worth 16x16 words: Transformers for image recognition at scale. *arXiv preprint arXiv:2010.11929*, 2020.

Alaaeldin El-Nouby, Gautier Izacard, Hugo Touvron, Ivan Laptev, Hervé Jegou, and Edouard Grave. Are large-scale datasets necessary for self-supervised pre-training? *arXiv preprint arXiv:2112.10740*, 2021.

Spyros Gidaris, Praveer Singh, and Nikos Komodakis. Unsupervised representation learning by predicting image rotations. *arXiv preprint arXiv:1803.07728*, 2018.

Priya Goyal, Dhruv Mahajan, Abhinav Gupta, and Ishan Misra. Scaling and benchmarking self-supervised visual representation learning. In *Proceedings of the ieee/cvf International Conference on computer vision*, pp. 6391–6400, 2019.

Priya Goyal, Mathilde Caron, Benjamin Lefaudeux, Min Xu, Pengchao Wang, Vivek Pai, Mannat Singh, Vitaliy Liptchinsky, Ishan Misra, Armand Joulin, et al. Self-supervised pretraining of visual features in the wild. *arXiv preprint arXiv:2103.01988*, 2021.

Jean-Bastien Grill, Florian Strub, Florent Altché, Corentin Tallec, Pierre Richemond, Elena Buchatskaya, Carl Doersch, Bernardo Avila Pires, Zhaohan Guo, Mohammad Gheshlaghi Azar, et al. Bootstrap your own latent-a new approach to self-supervised learning. *Advances in Neural Information Processing Systems*, 33:21271–21284, 2020.

Kaiming He, Haoqi Fan, Yuxin Wu, Saining Xie, and Ross Girshick. Momentum contrast for unsupervised visual representation learning. In *Proceedings of the IEEE/CVF conference on computer vision and pattern recognition*, pp. 9729–9738, 2020.

Kaiming He, Xinlei Chen, Saining Xie, Yanghao Li, Piotr Dollár, and Ross Girshick. Masked autoencoders are scalable vision learners. *arXiv preprint arXiv:2111.06377*, 2021.

Chunyuan Li, Jianwei Yang, Pengchuan Zhang, Mei Gao, Bin Xiao, Xiyang Dai, Lu Yuan, and Jianfeng Gao. Efficient self-supervised vision transformers for representation learning. *arXiv preprint arXiv:2106.09785*, 2021a.

Zhaowen Li, Zhiyang Chen, Fan Yang, Wei Li, Yousong Zhu, Chaoyang Zhao, Rui Deng, Liwei Wu, Rui Zhao, Ming Tang, et al. Mst: Masked self-supervised transformer for visual representation. *Advances in Neural Information Processing Systems*, 34:13165–13176, 2021b.

Yinhan Liu, Myle Ott, Naman Goyal, Jingfei Du, Mandar Joshi, Danqi Chen, Omer Levy, Mike Lewis, Luke Zettlemoyer, and Veselin Stoyanov. Roberta: A robustly optimized bert pretraining approach. *arXiv preprint arXiv:1907.11692*, 2019.

Ilya Loshchilov and Frank Hutter. Decoupled weight decay regularization. *arXiv preprint arXiv:1711.05101*, 2017.

Tomasz Malisiewicz, Abhinav Gupta, and Alexei A Efros. Ensemble of exemplar-svms for object detection and beyond. In *2011 International conference on computer vision*, pp. 89–96. IEEE, 2011.

Tomas Mikolov, Ilya Sutskever, Kai Chen, Greg S Corrado, and Jeff Dean. Distributed representations of words and phrases and their compositionality. *Advances in neural information processing systems*, 26, 2013.

Mehdi Noroozi and Paolo Favaro. Unsupervised learning of visual representations by solving jigsaw puzzles. In *European conference on computer vision*, pp. 69–84. Springer, 2016.

Aaron van den Oord, Yazhe Li, and Oriol Vinyals. Representation learning with contrastive predictive coding. *arXiv preprint arXiv:1807.03748*, 2018.

Alec Radford, Jong Wook Kim, Chris Hallacy, Aditya Ramesh, Gabriel Goh, Sandhini Agarwal, Girish Sastry, Amanda Askell, Pamela Mishkin, Jack Clark, et al. Learning transferable visual models from natural language supervision. In *International Conference on Machine Learning*, pp. 8748–8763. PMLR, 2021.

Pierre H Richemond, Jean-Bastien Grill, Florent Altché, Corentin Tallec, Florian Strub, Andrew Brock, Samuel Smith, Soham De, Razvan Pascanu, Bilal Piot, et al. Byol works even without batch statistics. *arXiv preprint arXiv:2010.10241*, 2020.

Chenxin Tao, Xizhou Zhu, Gao Huang, Yu Qiao, Xiaogang Wang, and Jifeng Dai. Siamese image modeling for self-supervised vision representation learning. *arXiv preprint arXiv:2206.01204*, 2022.

Yonglong Tian, Chen Sun, Ben Poole, Dilip Krishnan, Cordelia Schmid, and Phillip Isola. What makes for good views for contrastive learning? *Advances in Neural Information Processing Systems*, 33:6827–6839, 2020.

Hugo Touvron, Matthieu Cord, Matthijs Douze, Francisco Massa, Alexandre Sablayrolles, and Hervé Jégou. Training data-efficient image transformers & distillation through attention. In *International Conference on Machine Learning*, pp. 10347–10357. PMLR, 2021a.

Hugo Touvron, Matthieu Cord, Alexandre Sablayrolles, Gabriel Synnaeve, and Hervé Jégou. Going deeper with image transformers. In *Proceedings of the IEEE/CVF International Conference on Computer Vision*, pp. 32–42, 2021b.

Dmitry Ulyanov, Andrea Vedaldi, and Victor Lempitsky. Deep image prior. In *Proceedings of the IEEE conference on computer vision and pattern recognition*, pp. 9446–9454, 2018.

Ashish Vaswani, Noam Shazeer, Niki Parmar, Jakob Uszkoreit, Llion Jones, Aidan N Gomez, Łukasz Kaiser, and Illia Polosukhin. Attention is all you need. *Advances in neural information processing systems*, 30, 2017.

Chen Wei, Haoqi Fan, Saining Xie, Chao-Yuan Wu, Alan Yuille, and Christoph Feichtenhofer. Masked feature prediction for self-supervised visual pre-training. *arXiv preprint arXiv:2112.09133*, 2021.

Zhirong Wu, Yuanjun Xiong, Stella X Yu, and Dahua Lin. Unsupervised feature learning via non-parametric instance discrimination. In *Proceedings of the IEEE conference on computer vision and pattern recognition*, pp. 3733–3742, 2018.

Tete Xiao, Yingcheng Liu, Bolei Zhou, Yuning Jiang, and Jian Sun. Unified perceptual parsing for scene understanding. In *European Conference on Computer Vision*. Springer, 2018.

Richard Zhang, Phillip Isola, and Alexei A Efros. Colorful image colorization. In *European conference on computer vision*, pp. 649–666. Springer, 2016.

Richard Zhang, Phillip Isola, and Alexei A Efros. Split-brain autoencoders: Unsupervised learning by cross-channel prediction. In *Proceedings of the IEEE Conference on Computer Vision and Pattern Recognition*, pp. 1058–1067, 2017.

Nanxuan Zhao, Zhirong Wu, Rynson WH Lau, and Stephen Lin. Distilling localization for self-supervised representation learning. *arXiv preprint arXiv:2004.06638*, 2020a.

Nanxuan Zhao, Zhirong Wu, Rynson WH Lau, and Stephen Lin. What makes instance discrimination good for transfer learning? *arXiv preprint arXiv:2006.06606*, 2020b.

Bolei Zhou, Hang Zhao, Xavier Puig, Sanja Fidler, Adela Barriuso, and Antonio Torralba. Scene parsing through ade20k dataset. In *Proceedings of the IEEE Conference on Computer Vision and Pattern Recognition*, 2017.

Jinghao Zhou, Chen Wei, Huiyu Wang, Wei Shen, Cihang Xie, Alan Yuille, and Tao Kong. ibot: Image bert pre-training with online tokenizer. *arXiv preprint arXiv:2111.07832*, 2021.

## A Discussions on CaiT-Style Architecture

ExtreMA follows the CaiT-style transformer architecture Touvron et al. (2021b), where the class token is appended later in the attention blocks. We find that such design is critical for ExtreMA to stabilize learning, whereas the conventional ViT class token design failed to converge properly. Additionally, we also investigate a third option on using average pooling across tokens to aggregate the holistic representation. In Figure 5, we plot the training loss and the kNN classification accuracy for different class token designs. The ViT class token design leads to unstable optimization, and average pooling finds a representation shortcut. The CaiT-style architecture works as desired.

It remains as a limitation of this work to fully understand the training dynamics for the class token design. We hypothesize that the problem originates from the Siamese networks processing input sequences with very different lengths. This makes the learning of the class token representation harder, when it is processed throughout the network.

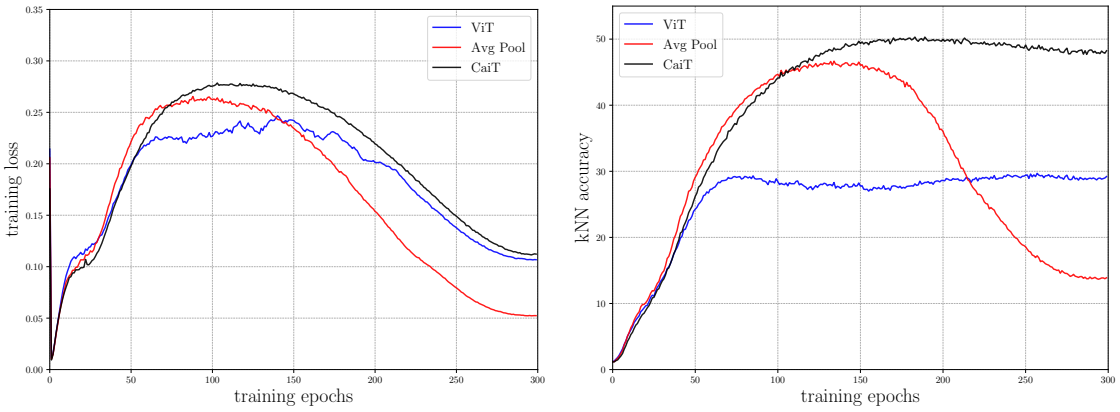


Figure 5: Training loss and kNN accuracy curves for three class token designs: ViT, average pooling, and CaiT. The network is trained with the ExtreMA objective with masking ratio 90% of 8 crops, using the ViT-small architecture.

## B Additional Comparisons of Locality Properties

We compare the performance on localization with other works, MAE / DINO / MoCo-v3. We use the [cls] token representation from these models. In Figure 6, we find that DINO performs favorably well, and that MAE / MoCo-v3 degrades the performance notably. MAE does not supervise an instance representation in the formulation, and hence its instance representation is weaker. MoCo-v3 suffers from the heavy use of spatial cropping augmentation, and DINO improves by using small local crops for localization.

## C Details of Evaluation Protocols

The evaluation protocols for end-to-end finetuning and linear probing largely follow BEiT and MAE. The hyper-parameter configurations are detailed in Table 12 and Table 13. We finetune ViT-Small models for 200 epochs and ViT-Base models for 100 epochs. We use a base learning rate 1e-3 and layer decay 0.75 for ImageNet1k pretrained models, and a slightly smaller learning rate 5e-4 and a smaller layer decay 0.65 for ImageNet22k pretrained models. The linear probing configuration is adopted consistently for all reported entries.

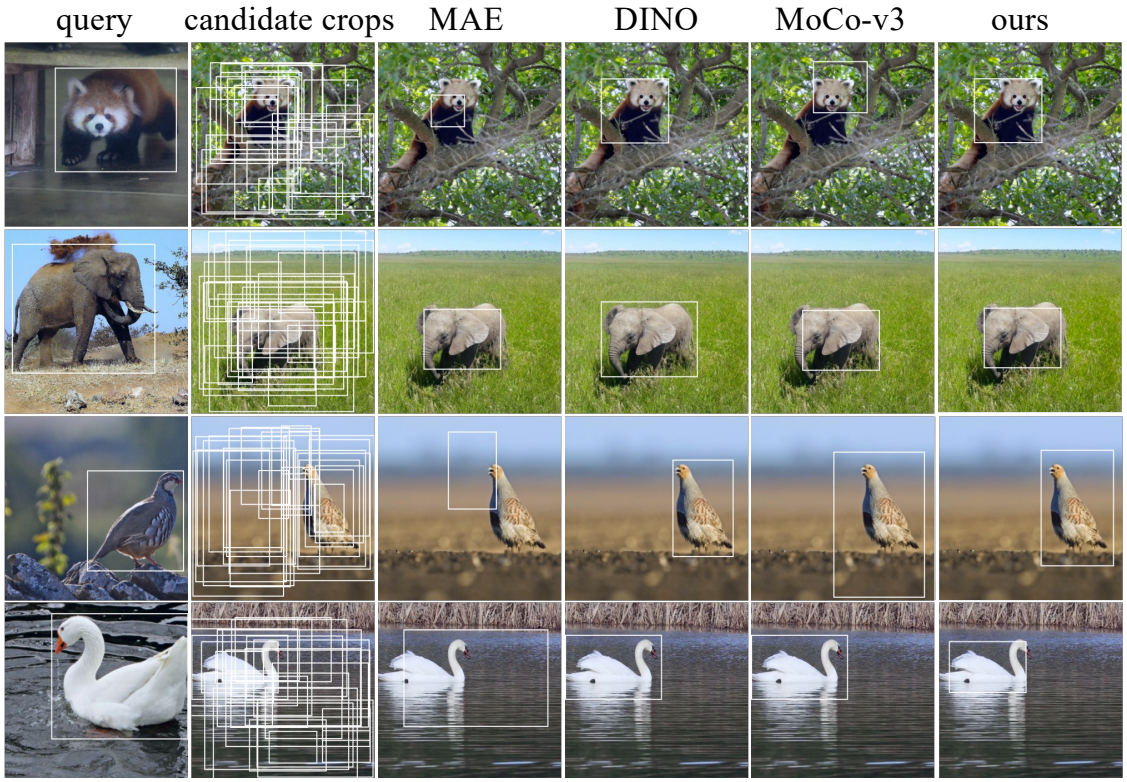


Figure 6: State-of-the-art comparisons with other models for localization.

Table 12: End-to-end fine-tuning protocol.

| config | value |
|---|---|
| optimizer | AdamW |
| base learning rate | 1e-3 |
| weight decay | 0.05 |
| optimizer momentum | $\beta_1, \beta_2$=0.9, 0.999 |
| layer-wise lr decay | 0.75 |
| batch size | 1024 |
| learning rate schedule | cosine decay |
| warmup epochs | 5 |
| training epochs | 200 (S), 100 (B) |
| augmentation | RandAug (9, 0.5) |
| label smoothing | 0.1 |
| mixup | 0.8 |
| cutmix | 1.0 |
| drop path | 0.1 |

Table 13: Linear probing protocol.

| config | value |
|---|---|
| optimizer | LARS |
| base learning rate | 0.1 |
| weight decay | 0 |
| optimizer momentum | 0.9 |
| batch size | 4096 |
| learning rate schedule | cosine decay |
| warmup epochs | 10 |
| training epochs | 90 |
| augmentation | RandomResizedCrop |

## D Additional Visualizations

We provide additional visualizations on the generative aspects of our model in Fig. 7, and attention maps of the distributed representations in Fig. 8. Both visualizations reveal properties of the distributed representations. These representations maintain accurate correspondences with the input tokens, while inferring meaningful semantic relationships among tokens.

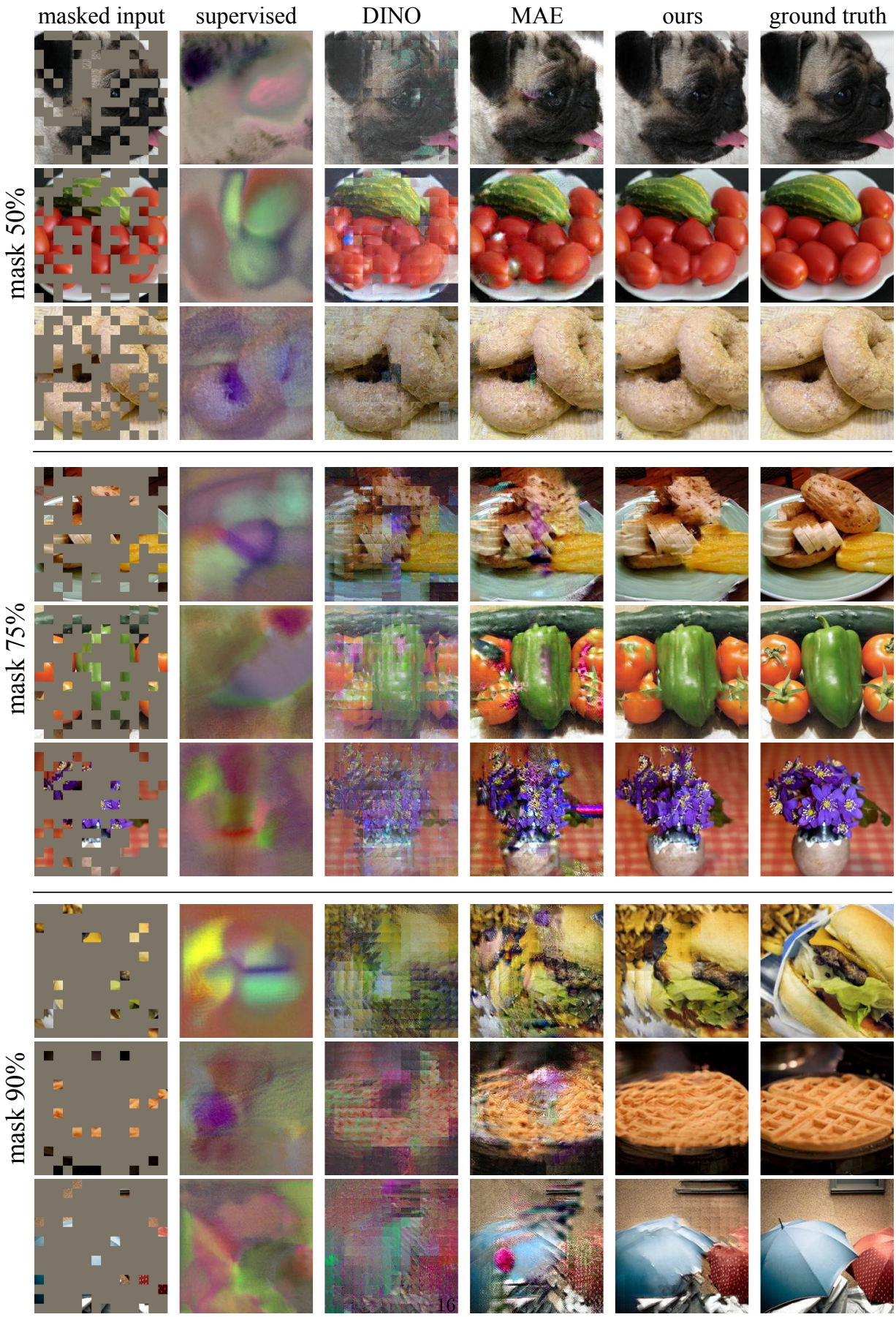


Figure 7: **Additional examples of inpainting at various masking ratios.**

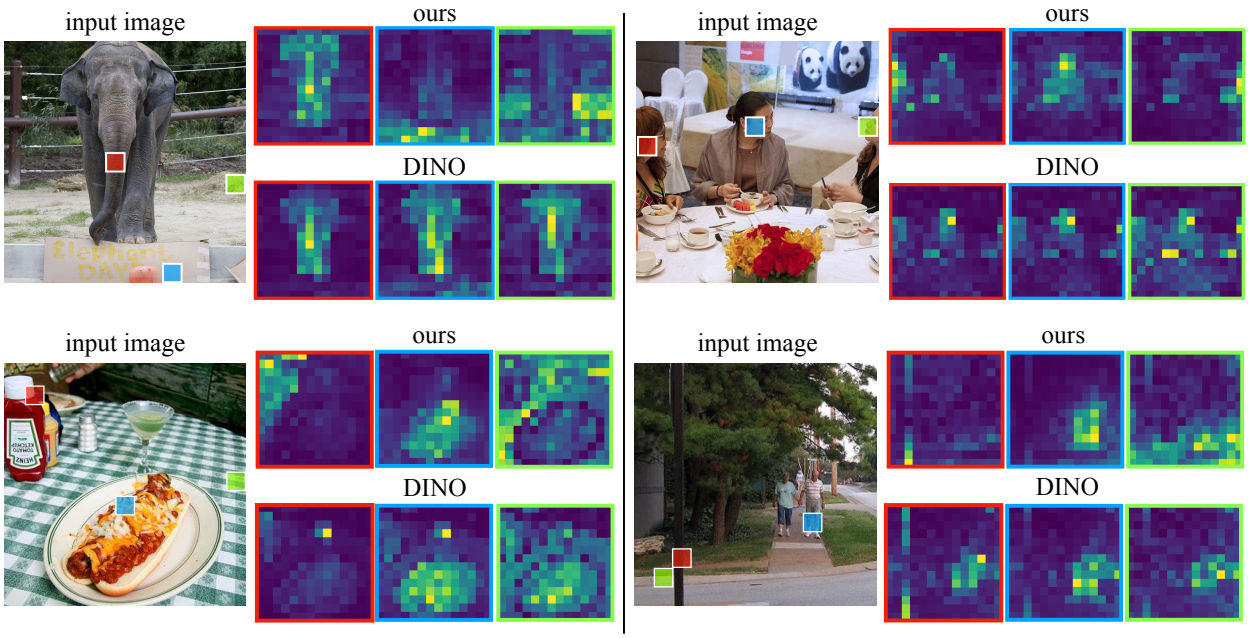


Figure 8: **Attention maps on the last layer of the ViT encoder.** We average the responses for 12 attention heads for visualization. Our model produces diverse and distributed attention maps, whereas DINO Caron et al. (2020) mainly attends to the foreground object, ignoring the others. The border color of the attention map corresponds to the colored query in the input image.